Fully Bayesian Differential Gaussian Processes through Stochastic Differential Equations

Jian Xu, Zhiqi Lin, Min Chen Fellow, IEEE, Junmei Yang, Delu Zeng, Member, IEEE, John Paisley

Abstract—Traditional deep Gaussian processes model the data evolution using a discrete hierarchy, whereas differential Gaussian processes (DIFFGPs) represent the evolution as an infinitely deep Gaussian process. However, prior DIFFGP methods often overlook the uncertainty of kernel hyperparameters and assume them to be fixed and time-invariant, failing to leverage the unique synergy between continuous-time models and approximate inference. In this work, we propose a fully Bayesian approach that treats the kernel hyperparameters as random variables and constructs coupled stochastic differential equations (SDEs) to learn their posterior distribution and that of inducing points. By incorporating estimation uncertainty on hyperparameters, our method enhances the model's flexibility and adaptability to complex dynamics. Additionally, our approach provides a timevarying, comprehensive, and realistic posterior approximation through coupling variables using SDE methods. Experimental results demonstrate the advantages of our method over traditional approaches, showcasing its superior performance in terms of flexibility, accuracy, and other metrics. Our work opens up exciting research avenues for advancing Bayesian inference and offers a powerful modeling tool for continuous-time Gaussian processes.

Index Terms—Differential Gaussian Process, Variational Inference, Stochastic Differential Equations

I. INTRODUCTION

Traditional Gaussian processes models [1] have limitations in handling non-Gaussian distributions, complex distributions, time series, and other challenging tasks. To address this, deep Gaussian processes (DGPs) have been introduced for more expressive representations. However, DGPs may face issues with degenerate models if individual GPs are not invertible [2], [3]. One approach to overcome these challenges is DIffGPs [4], which model data evolution in continuous time using stochastic differential equation systems. This allows for learning continuous-time transformations of the data, offering a more natural way to capture data dynamics compared to traditional methods. DIffGPs warp inputs through differential fields to generalize discrete layers into a dynamic system. The intuition of "warping" the inputs over time, as derived from the original DiffGP paper, is an extension of the concept of deep Gaussian processes in continuous layers. Similar to the

Jian Xu is with School of Computer Science, South China University of Technology in Guangdong Province, China. Email: 202311089192@mail.scut.edu.cn, minchen@ieee.org.

Junmei Yang, Delu Zeng are with the School of Electronic and Information Engineering at South China University of Technology in Guangdong Province, China. Email: dlzeng@scut.edu.cn, yjunmei@scut.edu.cn

John Paisley is with the Department of Electrical Engineering at Columbia University, New York, USA. Email: jwp2128@columbia.edu

Corresponding author: Delu Zeng, dlzeng@scut.edu.cn

transition from ResNet to neural ODEs, this approach aims to adapt and transform the input space progressively over time, allowing the model to better capture complex patterns and dependencies in the data.

The DIffGP methods [4] have been criticized for overlooking uncertainty in kernel hyperparameters, crucial for accurate modeling and reliable uncertainty estimation. The choice of covariance function in GPs significantly impacts the posterior distribution, highlighting the importance of selecting a proper covariance function [5], [6]. Model selection in GP modeling involves specifying covariance functions and selecting hyperparameters, typically done by maximizing the marginal likelihood or its lower bound. However, this approach faces challenges due to the non-convex nature of the marginal likelihood surface, especially with multiple modes and weakly identifiable hyperparameters. Maximizing the marginal likelihood may lead to overfitting and underestimation of prediction uncertainty, as gradient-based optimization is sensitive to initial values. Improved methods are needed to address these challenges in hyperparameter estimation for GP models.

In this work, we propose a fully Bayesian approach to Gaussian process regression, treating kernel hyperparameters as random variables and using coupled stochastic differential equations (SDEs) to learn their posterior distribution and that of inducing points. This method effectively addresses the nonconvexity of the marginal likelihood surface, providing robust parameter estimation. By incorporating uncertainty in hyperparameters through the posterior distribution, overfitting is avoided, and generalization to new data is enhanced. Bayesian methods offer a comprehensive understanding of parameter estimation by capturing inherent uncertainty, improving model reliability and adaptability.

Extending the Bayesian treatment of hyperparameters to a hierarchical framework presents challenges in computing posterior distributions, leading to increased complexity. We introduce a novel methodology using SDEs to learn the posterior distribution of hyperparameters and inducing points, capturing their uncertainty effectively. By integrating Bayesian inference with SDEs, our approach enhances model adaptability and robustness in capturing system dynamics.

Our work introduces a novel network architecture that not only enhances the expressiveness of DIffGPs but also integrates the uncertainty of kernel parameters and inducing point distributions into a fully Bayesian inference framework, incorporating their time-correlated posterior SDEs. By leveraging state-of-the-art SDE gradient estimators, such as those in [7], [8], [9], [10], we demonstrate the effectiveness

of approximate inference by maximizing our modified variational lower bound, significantly improving the scalability of gradient-based variational inference compared to previous studies. Computation of the output layer state is simplified using a black-box adaptive SDE solver, streamlining the modeling process and enhancing the efficiency of our proposed methodology.

Our approach offers two distinct advantages over previous DIffGPs models: i). Incorporating the uncertainty of inducing points and kernel hyperparameters within a fully Bayesian framework enhances flexibility and adaptability in capturing complex dynamics. ii). By expanding the neural network that parameterizes the dynamics of the approximate posterior, the variational posterior can be made highly expressive. This enables accurate approximation of the true posterior, leading to a more comprehensive and realistic posterior approximation and preventing overfitting.

Experimental evaluation showcases the superiority of our proposed method over traditional approaches in terms of flexibility, accuracy, and other relevant metrics. Our contributions are outlined as follows:

- We introducing a fully Bayesian approach that treats kernel hyperparameters as random variables and utilizes coupled stochastic differential equations (SDEs) to learn their posterior distribution and that of inducing points for DIFFGPs, enhancing model flexibility and adaptability to complex dynamics by incorporating estimation uncertainty on hyperparameters.
- Using advanced SDE gradient estimators, our approach scales up gradient-based variational inference significantly. The utilization of a black-box adaptive SDE solver for computing the output layer underpins our commitment to effective and innovative model computation.
- Experimental results showcase the advantages of our method over traditional approaches, demonstrating superior performance in terms of flexibility, accuracy, and other metrics.

II. MODEL

A. Gaussian Processes and Sparse Representation

Gaussian processes (GPs) are powerful probabilistic models that define a distribution over functions. Given a collection of input points $\mathbf{X} = \{\mathbf{x}_1, \dots, \mathbf{x}_N\}^\top \in \mathbb{R}^{N \times D}$, where $\mathbf{x}_i \in \mathbb{R}^D$, a GP specifies a joint Gaussian distribution over the corresponding function values $\mathbf{f} = \{f(\mathbf{x}_1), \dots, f(\mathbf{x}_N)\}^\top \in \mathbb{R}^N$. The fundamental property of GPs is that the outputs at different points correlate based on their similarity, as measured by a kernel function $k(\mathbf{x}, \mathbf{x}')$, as described by Rasmussen and Williams [1].

Traditionally, a zero-mean Gaussian process prior is defined on a function $f(\mathbf{x})$ over vector inputs $\mathbf{x} \in \mathbb{R}^D$:

$$f(\mathbf{x}) \sim \mathcal{GP}(0, k(\mathbf{x}, \mathbf{x}')),$$

where $k(\mathbf{x}, \mathbf{x}')$ is the kernel function, and it captures the covariance between function values at different inputs.

To handle large datasets effectively, we can employ sparse Gaussian processes that utilize a small set of inducing or landmark variables. These inducing variables $\mathbf{u}=$

 $\{u_1,\ldots,u_M\}^{\top}\in\mathbb{R}^M$, where M is much smaller than N, are chosen from the dataset. By conditioning the GP prior on these inducing variables \mathbf{u} and their corresponding locations $\mathbf{Z}=\{\mathbf{z}_1,\ldots,\mathbf{z}_M\}^{\top}$, we can obtain posterior predictions at the data points.

The sparse GP posterior predictions, given the inducing variables \mathbf{u} and their locations \mathbf{Z} , are given by:

$$\begin{aligned} \mathbf{f} \mid \mathbf{u}, \mathbf{Z} \sim \mathcal{N}(\mathbf{Q}\mathbf{u}, \mathbf{K_{XX}} - \mathbf{Q}\mathbf{K_{ZZ}}\mathbf{Q}^{\top}) \\ \mathbf{u} \sim \mathcal{N}(\mathbf{0}, \mathbf{K_{ZZ}}), \end{aligned}$$

where $\mathbf{Q} = \mathbf{K}_{\mathbf{XZ}}(\mathbf{K}_{\mathbf{ZZ}} + \sigma_n^2 \mathbf{I})^{-1}$ is the matrix of the coefficients relating the inducing variables to the function values, n in σ_n refers to the position of the sample point, $\mathbf{K}_{\mathbf{XX}}$ is the kernel matrix between the data points, $\mathbf{K}_{\mathbf{ZZ}}$ is the kernel matrix between the inducing points, $\mathbf{K}_{\mathbf{XZ}}$ is the kernel matrix between the data points and the inducing points, and σ_n^2 is the noise variance of the observations.

The main inference problems for Gaussian Processes (GPs) are related to the inducing points \mathbf{Z} , inducing variables \mathbf{u} , and the kernel hyperparameters λ . For instance, if we choose the classic Gaussian kernel, the formula for the kernel is:

$$k(\mathbf{x}, \mathbf{x}') = \sigma_f^2 \exp(-\frac{\|\mathbf{x} - \mathbf{x}'\|^2}{2l^2})$$
 (1)

In classical inference methods, VI [11] and Markov Chain Monte Carlo (MCMC) [12] have been widely successful. By incorporating sparse representation through inducing variables, we can effectively model and make predictions in large-scale datasets using Gaussian processes.

B. Continuous-Time Gaussian Processes

The continuous-time deep learning paradigm introduced by [4] focuses on a model called DIFFGP, which is a continuous-time deep Gaussian process model through infinite, infinitesimal differential compositions. In DIFFGP models, the input data is transformed using a stochastic differential equation (SDE) flow to obtain transformed inputs \mathbf{X}_T , which are then used for model fitting after a predefined time T. The parameter T determines the length of the flow and the system's capacity, similar to the number of layers in standard deep GPs or deep neural networks.

In this paradigm, the inputs are redefined as temporal functions $\mathbf{x}: \mathcal{T} \to \mathbb{R}^D$ over time, where state paths \mathbf{x}_t over time $t \in \mathcal{T} = \mathbb{R}_+$ emerge. The observed inputs $\mathbf{x}_{i,0}$ correspond to initial states. The task is to classify or regress the final data points $\mathbf{X}_T = (\mathbf{x}_{1,T}, \dots, \mathbf{x}_{N,T})^{\top}$ after T time of an SDE flow using a predictor Gaussian process. In above notation, the first index represents the dimension of the sample points, indicating the number of sample particles. The second index represents the dimension of the discrete time points. The predictor is denoted as $g(\mathbf{x}_T)$ and is assumed to follow a Gaussian process prior with zero mean and a covariance function $K(\mathbf{x}_T, \mathbf{x}_T')$. When T = 0, the framework reduces to a conventional Gaussian process.

The prediction depends on the final dataset X_T structure, determined by the SDE flow dx_t from the original data X. We consider SDE flows of Ito type

$$d\mathbf{x}_{t} = \boldsymbol{\mu}\left(\mathbf{x}_{t}\right)dt + \sqrt{\Sigma\left(\mathbf{x}_{t}\right)}dW_{t}$$
 (2)

where

$$\begin{aligned} \boldsymbol{\mu}(\mathbf{x}_t) &= \mathbf{K}_{\mathbf{x}\mathbf{Z}}\mathbf{K}_{\mathbf{Z}\mathbf{Z}}^{-1}\operatorname{vec}\left(\mathbf{U}\right) \\ \boldsymbol{\Sigma}(\mathbf{x}_t) &= \mathbf{K}_{\mathbf{x}\mathbf{x}} - \mathbf{K}_{\mathbf{x}\mathbf{Z}}\mathbf{K}_{\mathbf{Z}\mathbf{Z}}^{-1}\mathbf{K}_{\mathbf{Z}\mathbf{x}} \end{aligned}$$

are the vector-valued Gaussian process conditioned on inducing variable $\mathbf{U} = (\mathbf{u}_1, \dots, \mathbf{u}_M)^{\top}$ defining function values $\mathbf{f}(\mathbf{z})$ at inducing states $\mathbf{Z} = (\mathbf{z}_1, \dots, \mathbf{z}_M)$. In Equation (2), the size of \mathbf{U} is $M \times D$, corresponding to a multi-output Gaussian process where the output dimension is D. Consequently, the dimension of $\mathbf{K}_{\mathbf{Z}\mathbf{Z}}$ is $MD \times MD$. This is a block matrix of matrix-valued kernels, reflecting the dependencies between the M inducing points and the D output dimensions.

The transformation process can be simulated using an SDE solver, such as Euler discretization [13]:

$$\mathbf{x}_T = \mathbf{x}_0 + \int_0^T \boldsymbol{\mu}(\mathbf{x}_t) dt + \int_0^T \sqrt{\Sigma(\mathbf{x}_t)} dW_t, \quad (3)$$

The DIFFGP model, which captures the time evolution and dynamics of data in a continuous manner, offers a more natural and flexible approach compared to traditional discrete-layered approaches like Deep GPs [14], [15]. However, the original DIFFGP model has limitations. For example, it treats the kernel parameters as point estimates and does not consider their uncertainty or fully incorporate a Bayesian perspective. Additionally, it does not account for the temporal variability of the kernel parameters and inducing points, similar to how each layer in a deep GP has its own kernel parameters and inducing points. In the following section, we will introduce a new fully Bayesian framework that addresses these issues by utilizing recent advancements in SDE theory and its connection to variational inference.

III. FULLY BAYESIAN VARIATIONAL INFERENCE

A. Modeling Uncertainty in Kernel Hyperparameters and Inducing Points

Within the realm of Gaussian process (GP) regression, the effectiveness of the model is intricately tied to the judicious selection of kernel hyperparameters and inducing points, a task renowned for its inherent complexity. The pursuit of optimal values for these parameters presents a formidable challenge that demands a strategic approach. In response to this challenge, our proposed methodology advocates for the adoption of a comprehensive Bayesian framework that explicitly acknowledges and encompasses the uncertainty inherent in the kernel hyperparameters and inducing points. By immersing this uncertainty into the very core of the inference process, we cultivate a model that not only exhibits heightened resilience but also demonstrates exceptional adaptability, poised to navigate the intricate nuances of the data landscape with enhanced agility and robustness.

In the generating process of the model, we assume that the kernel hyperparameters λ_t , inducing points \mathbf{Z}_t , and inducing variables \mathbf{U}_t are drawn from certain prior distributions. These hyperparameters control the behavior of the Gaussian process model and are crucial for determining the smoothness and flexibility of the model. The inducing points \mathbf{Z}_t are any set of points within the input space that can be optimized to approximate the function values at all input points. The

inducing variables U_t are the corresponding function values at the inducing points.

Given these prior distributions, the model generates the observed data \mathbf{X} and \mathbf{y} by drawing samples from the Gaussian process defined by the kernel function with the hyperparameters λ_t and the inducing variables \mathbf{U}_t . For example, in the classic Gaussian kernel, $\lambda = \{\sigma_f, l\}$. The posterior distribution of the hyperparameters, inducing points, and inducing variables can then be estimated based on the observed data using Bayesian inference techniques. This allows us to make predictions and infer the underlying structure of the data based on the Gaussian process model,

Prior over hyperparameters $\lambda_t \sim p(\lambda_t)$ Prior over inducing points $\mathbf{Z}_t \sim p(\mathbf{Z}_t)$ Prior over inducing variables $\mathbf{U}_t \sim \mathcal{GP}(0, K(\mathbf{Z}_t, \mathbf{Z}_t'))$ Model forward SDE $d\mathbf{x}_t = \boldsymbol{\mu}(\mathbf{x}_t) dt + \sqrt{\Sigma(\mathbf{x}_t)} dW_t$ Predictor Gaussian process $\mathbf{g} \sim \mathcal{GP}(0, K(\mathbf{x}_T, \mathbf{x}_T'))$ Data likelihood $\mathbf{y} \mid \mathbf{g} \sim \mathcal{N}(\mathbf{g}, \sigma_n^2 \mathbb{I})$

Inspired by the ANODEV2 method [16], which extends a complex ODE model for evolving neural network parameters, we view the hyperparameters λ_t and inducing points \mathbf{Z}_t as prior processes that evolve over time, in contrast to traditional fully-GP models and previous works like DIFFGPs. This approach departs from the fixed hyperparameters assumption and allows for a more dynamic modeling of the parameter evolution. Drawing parallels to evolutionary computing methods such as HyperNEAT [17], Compressed Weight Search [18], and Hypernetworks [19], which employ secondary networks to generate parameters for the main network, our approach extends this concept to parameter evolution in GP-SDE models. By adopting a Bayesian perspective, we aim to capture the time-varying distribution of hyperparameters, thereby enhancing the flexibility and adaptability of our model.

We can apply the concept of amortized variational inference, as introduced in the works of [20], [21], [5], to optimize the factorized approximate posterior distribution $q(\lambda_t, \mathbf{Z}_t, \mathbf{U}_t) = q(\lambda_t)q(\mathbf{Z}_t)q(\mathbf{U}_t)$. This requirement is met by employing the mean-field assumption, where the posterior is approximated as a product of several independent factors. The goal is to minimize the Kullback-Leibler (KL) divergence between this approximate posterior and the true posterior distribution. This optimization objective is equivalent to maximizing the Evidence Lower Bound (ELBO), which serves as a lower bound on the marginal likelihood of the data under the model. By maximizing the ELBO, we can efficiently approximate the true posterior distribution and make accurate inference about the model's parameters and latent variables,

$$\log p(\mathbf{y})$$

$$\geq \mathbb{E}_{q(\boldsymbol{\lambda}_{0:T})q(\mathbf{Z}_{0:T})q(\mathbf{U}_{0:T})p(\mathbf{x}_{T}|\boldsymbol{\lambda}_{0:T},\mathbf{Z}_{0:T},\mathbf{U}_{0:T})p(\mathbf{g}|\mathbf{x}_{T})}[\log p(\mathbf{y} \mid \mathbf{g})]$$

$$-KL(q(\boldsymbol{\lambda}_{0:T}) \parallel p(\boldsymbol{\lambda}_{0:T})) - KL(q(\mathbf{Z}_{0:T}) \parallel p(\mathbf{Z}_{0:T}))$$

$$-KL(q(\mathbf{U}_{0:T}) \parallel p(\mathbf{U}_{0:T}))$$
(5)

where $\lambda_{0:T}$, $\mathbf{Z}_{0:T}$, and $\mathbf{U}_{0:T}$ represent the trajectory paths of λ_t , \mathbf{Z}_t , and \mathbf{U}_t respectively. Next, we show how to do efficient variational inference in SDE models, and optimize the marginal log-likelihood to fit both prior hyperparameters

and the parameters of a tractable approximate posterior over functions.

B. Approximate Posterior through Latent Stochastic Differential Equations

To perform posterior inference in our model, we leverage latent stochastic differential equations [22], [7], [23], [24]. These SDEs provide a principled and flexible framework for modeling complex temporal dynamics. In particular, we can parameterize both a prior over functions and an approximate posterior using coupled SDEs in the following system of differential equations.

$$\begin{cases}
d\lambda_{t} = h_{\theta_{\lambda}}(\lambda_{t}, t) dt + l_{\lambda}(\lambda_{t}, t) dW_{t}, (\text{prior}) \\
d\lambda_{t} = h_{\phi_{\lambda}}(\lambda_{t}, t) dt + l_{\lambda}(\lambda_{t}, t) dW_{t}, (\text{approx.posterior})
\end{cases}$$

$$\begin{cases}
d\mathbf{Z}_{t} = h_{\theta_{z}}(\mathbf{Z}_{t}, t) dt + l_{z}(\mathbf{Z}_{t}, t) dW_{t}, (\text{prior}) \\
d\mathbf{Z}_{t} = h_{\phi_{z}}(\mathbf{Z}_{t}, t) dt + l_{z}(\mathbf{Z}_{t}, t) dW_{t}, (\text{approx.posterior})
\end{cases}$$
(6)

The difference between the prior and posterior processes lies solely in their drift terms. Similar to classical Bayesian analysis, the parameters of the prior SDE can be set to simple, fixed values, such as constants or basic affine transformations, while the drift term of the posterior SDE is parameterized by a fully connected neural network. This allows us to compute the KL divergence between the prior and posterior SDEs using Girsanov's theorem [25]. We apply this approach to both \mathbf{Z} and $\boldsymbol{\lambda}$ to ensure that our model retains fully Bayesian properties. Although we currently assume the drift term to be a simple function, it is also feasible to employ complex networks to learn the prior, a direction we intend to explore in future work.

For instance, in the context of an Ornstein-Uhlenbeck (OU) prior stochastic differential equation (SDE), we specify fixed prior drift coefficients as $h_{\theta_{\lambda}} = -\lambda_t$ and $h_{\theta_z} = -\mathbf{Z}_t$, along with fixed prior diffusion coefficients as $l_{\lambda} = \sigma_{\lambda} \mathbb{I}$ and $l_z = \sigma_z \mathbb{I}$. We choose to employ the OU process due to its simplicity and well-understood properties. This process can be represented by the following SDE:

$$d\lambda_t = -\lambda_t dt + \sigma_{\lambda} \mathbb{I} \ dW_t, (\text{prior})$$

$$d\mathbf{Z}_t = -\mathbf{Z}_t dt + \sigma_z \mathbb{I} \ dW_t, (\text{prior})$$
(7)

For the approximate posterior processes of λ_t and \mathbf{Z}_t , we also employ an SDE representation, where $h_{\phi_{\lambda}}$ and h_{ϕ_z} are parameterized neural networks, and all drift and diffusion functions are Lipschitz continuous. With these drifts, the approximate posterior process will generally have nonGaussian, non-factorized marginals. It may seem very restrictive to assume that the diffusion terms of the prior and posterior are identical in Eq. (6). However, previous results from the Neural SDE literature demonstrate that any posterior can be approximated with arbitrary closeness using such a functional form given a sufficiently expressive drift process [26], [10], [7], [24].

Then the Kullback-Leibler (KL) divergence between these distributions is finite and can be estimated by sampling paths from the posterior process [22], [7]. According to Girsanov's theorem [25], an essential result in stochastic calculus, it states how the probability measures change under a change of drift in stochastic processes. With respect to our context, Girsanov's

theorem allows us to express the Evidence Lower Bound (ELBO) in a concise and insightful manner, capturing the essence of the relationship between the true and approximate distributions in a probabilistic framework,

$$\log p(\mathbf{y})$$

$$\geq \mathbb{E}_{q(\boldsymbol{\lambda}_{0:T})q(\mathbf{Z}_{0:T})q(\mathbf{U}_{0:T})p(\mathbf{x}_{T}|\boldsymbol{\lambda}_{0:T},\mathbf{Z}_{0:T},\mathbf{U}_{0:T})p(\mathbf{g}|\mathbf{x}_{T})}[\log p(\mathbf{y} \mid \mathbf{g})]$$

$$-\frac{1}{2} \int_{0}^{T} \mathbb{E}_{q(\boldsymbol{\lambda}_{t})} |u_{\lambda}(\boldsymbol{\lambda}_{t},t)|^{2} dt$$

$$-\frac{1}{2} \int_{0}^{T} \mathbb{E}_{q(\mathbf{Z}_{t})} |u_{z}(\mathbf{Z}_{t},t)|^{2} dt - KL(q(\mathbf{U}_{0:T}) \parallel p(\mathbf{U}_{0:T}))$$
(8)

where

$$u_{\lambda}(\boldsymbol{\lambda}_{t}, t) = l_{\lambda}(\boldsymbol{\lambda}_{t}, t)^{-1} \left(h_{\theta_{\lambda}}(\boldsymbol{\lambda}_{t}, t) - h_{\phi_{\lambda}}(\boldsymbol{\lambda}_{t}, t) \right),$$

$$u_{z}(\mathbf{Z}_{t}, t) = l_{z}(\mathbf{Z}_{t}, t)^{-1} \left(h_{\theta_{z}}(\mathbf{Z}_{t}, t) - h_{\phi_{z}}(\mathbf{Z}_{t}, t) \right)$$

 $l_{\lambda}(\lambda_t,t)^{-1}$ and $l_z(\mathbf{Z}_t,t)^{-1}$ are the left inverse, and the expectation is taken over the approximate posterior process defined by Eq. (6). The functions u_{λ} and u_z need to fulfill the Novikov condition [7], which ensures that the drift and diffusion terms of the SDE are well-defined and that the process remains consistent with the requirements of stochastic calculus.

All estimates of stochastic differential equation (SDE) paths and gradients are simulated and computed using cutting-edge SDE solvers, as outlined in the work by [7]. Furthermore, to address large-scale data challenges efficiently, we can utilize mini-batch surrogates for likelihood optimization. This approach harnesses concepts from backpropagation introduced by [27] and stochastic optimization techniques such as those discussed by [28], [29], [15]. By employing mini-batch surrogates, we can effectively optimize likelihood functions for models handling significant amounts of data while retaining computational efficiency.

$$\log p\left(\mathbf{y}|\mathbf{g}\right) = \sum_{i=1}^{N} \log p\left(y_i|\mathbf{g}\right) \approx \frac{N}{B} \sum_{i=1}^{B} \log p\left(y_i|\mathbf{g}\right)$$
(9)

For variational inference of the inducing variable U_t , we follow the approach of previous work [4], by assuming that its posterior is a Gaussian distribution.

$$q\left(\mathbf{U}_{t}\right) = \mathcal{N}\left(\boldsymbol{m}_{t}, \boldsymbol{S}_{t}\right) \tag{10}$$

What sets this work apart from prior research is that m_t and S_t are time-dependent networks while in the original DiffGP, this term is modeled as a constant. We aim to characterize the dynamical system of the inducing variables over time. Since the fact that the Kullback-Leibler divergence between two Gaussian distributions is analytical, the expression $KL\left(q\left(\mathbf{U}_t\right)\parallel p\left(\mathbf{U}_t\right)\right)$ can be explicitly represented as,

$$KL\left(q\left(\mathbf{U}_{0:T}\right) \parallel p\left(\mathbf{U}_{0:T}\right)\right) = \int_{0}^{T} \mathbb{E}_{q\left(\mathbf{U}_{t}, \boldsymbol{\lambda}_{t}, \mathbf{Z}_{t}\right)} \log \frac{q\left(\mathbf{U}_{t}\right)}{p\left(\mathbf{U}_{t}\right)} dt$$

$$= \frac{1}{2} \int_{0}^{T} \mathbb{E}_{q\left(\boldsymbol{\lambda}_{t}, \mathbf{Z}_{t}\right)} \begin{pmatrix} Tr\left(K_{\mathbf{Z}_{t}\mathbf{Z}_{t}}^{-1} \mathbf{S}_{t}\right) + \boldsymbol{m}_{t}^{T} K_{\mathbf{Z}_{t}\mathbf{Z}_{t}}^{-1} \boldsymbol{m}_{t} - M \\ + \ln \frac{\det\left(K_{\mathbf{Z}_{t}\mathbf{Z}_{t}}\right)}{\det\left(S_{t}\right)} \end{pmatrix} dt$$

$$= \frac{1}{2} \int_{0}^{T} \mathbb{E}_{q\left(\boldsymbol{\lambda}_{t}, \mathbf{Z}_{t}\right)} \begin{pmatrix} Tr\left(K_{\mathbf{Z}_{t}\mathbf{Z}_{t}}^{-1} \mathbf{S}_{t}\right) + \mathbf{m}_{t}^{T} K_{\mathbf{Z}_{t}\mathbf{Z}_{t}}^{-1} \boldsymbol{m}_{t} - M \\ + \ln \frac{\det\left(K_{\mathbf{Z}_{t}\mathbf{Z}_{t}}\right)}{\det\left(S_{t}\right)} \end{pmatrix} dt$$

$$= \frac{1}{2} \int_{0}^{T} \mathbb{E}_{q\left(\boldsymbol{\lambda}_{t}, \mathbf{Z}_{t}\right)} \begin{pmatrix} Tr\left(K_{\mathbf{Z}_{t}\mathbf{Z}_{t}}^{-1} \mathbf{S}_{t}\right) + \mathbf{m}_{t}^{T} K_{\mathbf{Z}_{t}\mathbf{Z}_{t}}^{-1} \boldsymbol{m}_{t} - M \\ + \ln \frac{\det\left(K_{\mathbf{Z}_{t}\mathbf{Z}_{t}}\right)}{\det\left(S_{t}\right)} \end{pmatrix} dt$$

Since U_t has already been integrated out, there is no need for an expectation with respect to U_t . However, the expectations with respect to Z_t and λ_t are still necessary.

C. Simulation and Predictions

By combining Eq. (2) and Eq. (6), we can derive:

$$d\begin{pmatrix} \mathbf{x}_{t} \\ \boldsymbol{\lambda}_{t} \\ \mathbf{Z}_{t} \end{pmatrix} = \begin{pmatrix} \boldsymbol{\mu}(\mathbf{x}_{t}) \\ h_{\phi_{\lambda}}(\boldsymbol{\lambda}_{t}, t) \\ h_{\phi_{z}}(\mathbf{Z}_{t}, t) \end{pmatrix} dt + \begin{pmatrix} \sqrt{\Sigma}(\mathbf{x}_{t}) \\ l_{\lambda}(\boldsymbol{\lambda}_{t}, t) \\ l_{z}(\mathbf{Z}_{t}, t) \end{pmatrix} dW_{t}$$
(12)

By leveraging advanced SDE solvers for state trajectory approximation, we can effectively perform stochastic gradient estimation for optimizing Eq. (8). This technique enhances our understanding of the model's loss function and enables more efficient optimization. Integrating Bayesian methodologies for hyperparameters and inducing points with dynamic SDE posterior estimation leads to a more flexible and expressive posterior estimation for DIFFGPs. This advancement improves the model's adaptability in capturing complex system dynamics and enhances predictive capabilities, providing a powerful tool for robust and informed model predictions.

D. Related Work

a) Sparse GPs: Sparse Gaussian Processes are an extension of GPs that address scalability issues in modeling large datasets. Traditional GPs involve inverting the covariance matrix, which becomes computationally expensive as the size of the dataset increases. Sparse GPs¹ alleviate this issue by introducing a smaller set of "inducing points" that approximate the latent function properties over the entire dataset. By assuming a joint distribution over the function values at the inducing points and the entire data points, Sparse GPs can approximate the true GP model while significantly reducing the computational complexity. Sparse GPs have gained popularity in various applications, including machine learning [11], robotics [30], and computer vision [31], where dealing with large datasets is common. Modeling and inference with Sparse GPs have evolved considerably over the last few years with key contributions in the direction of scalability to virtually any number of datapoints and generality within automatic differentiation frameworks [32], [33], [34]. This has been possible thanks to the combination of stochastic variational inference techniques [29] with representations based on inducing variables [35], [36], [11]. These advancements have now made GPs attractive to a variety of applications and likelihoods [32], [37], [38], [39]. However, it is worth noting that Sparse GPs still require selecting the appropriate hyperparameters and inducing points, which can be challenging in some cases.

b) Fully bayesian GPs: The key distinction between Fully Bayesian GPs and traditional sparse Gaussian Processes lies in their modeling approach towards kernel hyperparameters. In traditional sparse Gaussian Processes, kernel hyperparameters are considered fixed or optimized model parameters. This means that during the modeling process, one needs to select a set of optimal hyperparameter values to fit the training data. While this approach can yield good results when the training data is abundant and of high quality, selecting appropriate hyperparameter values can become challenging, especially in situations with scarce or nonlinear data.

Fully Bayesian GPs treat kernel hyperparameters as random variables and introduce prior distributions to represent their uncertainty. This means that Fully Bayesian GPs no longer rely on fixed hyperparameter values but instead model the range of possible hyperparameter values and update their prior distributions based on the posterior distribution from the observed data. This approach enables the estimation of the true values of hyperparameters and their uncertainties using Bayesian inference, allowing for better adaptation to the data.

Fully Bayesian Gaussian processes have been extensively utilized by numerous researchers, resulting in the emergence of several variant approaches. In early studies, [40], [41] investigated the use of Hamiltonian Monte Carlo (HMC) methods to perform integration over covariance hyperparameters in the regression setting. [42] extended the application of HMC methods to the classification setting. They employed HMC for sampling in the hyperparameter space and utilized the Laplace approximation to compute the integral over function values. [43], [44] focused on MCMC schemes to sample covariance hyperparameters in conjunction with latent function values, mainly mitigating the coupling effect through reparameterisation. [12] considered joint sampling of inducing variables and hyperparameters from the optimal variational posterior distribution while [45] considered inference schemes for fully Bayesian sparse GPs in a streaming setting. The technique introduced by [5] incorporates Variational Inference (VI) into Fully Bayesian GPs, approximating the posterior over hyperparameters with a factorized Gaussian distribution (mean-field approximation). More recently, [46] modified the generative model by adding a prior over the inducing inputs, and performed inference using SG-HMC over the joint kernel hyperparameters λ , inducing points **Z**, inducing variables **U** space. Subsequently, [6] extended this method to a doubly collapsed bound, which analytically selected the optimal distribution over the inducing points.

c) GPs with deep architectures: We will also focus on the utilization of deep structures in GPs, specifically Deep Gaussian Processes (DGPs) and Differential Gaussian Processes (DIFFGPs) consisting of discrete layers and continuous layers. DGP [14] is a model composed of multiple layers of Gaussian processes. Each layer is a Gaussian process model used to model the nonlinear relationships in intermediate layers. The output layer of the DGP model provides the final prediction. In addition to traditional Bayesian inference methods, DGP introduces several new inference techniques. DSVI [15] introduced stochastic variational inference to handle largescale data and learn the distribution of model parameters. SGHMC [47] is a model that uses Hamiltonian Monte Carlo method for inference in deep Gaussian processes. This method incorporates stochastic gradients for learning, allowing for large-scale data processing during the inference process. IPVI [48] constructed an approximate posterior by introducing Nash equilibrium. NOVI [49] is a method that uses neural networks and score-based approaches to approximate the complex posterior distribution in DGPs. Unlike traditional DGP methods that focus on iterative function mappings, DIFFGPs [4] utilized SDEs to characterize continuous-depth Gaussian processes. By transforming the GP modeling into a continuous-time

¹In this paper, the term "Sparse GPs" refers to the method of using sparse inducing points, distinguishing it from other forms of representation.

	Method name	Sparse	Single-layer or deep architectures	Time-varying hyperparameters	U	λ	\mathbf{z}	Inference	Reference
Sparse GP	FITC-SVGP	√	Single-layer	N/A	Bayesian estimation	Point estimation	Point estimation	VI	[35]
sparse Gr	SVGP	✓	Single-layer	N/A	Bayesian estimation	Point estimation	Point estimation	SVI	[11]
Ell I CD	SMCMC-GP	√	Single-layer	N/A	Bayesian estimation	Bayesian estimation	Point estimation	MCMC	[12]
Fully bayesian GP	SSGP	✓	Single-layer	N/A	Bayesian estimation	Bayesian estimation	Point estimation	Streaming variational Bayes	[56]
	Fully Bayesian GPR	✓	Single-layer	N/A	Bayesian estimation	Bayesian estimation	Point estimation	VI/HMC	[5]
	BSGP	✓	Single-layer	N/A	Bayesian estimation	Bayesian estimation	Bayesian estimation	SG-HMC	[46]
	SGPR + HMC	✓	Single-layer	N/A	Bayesian estimation	Bayesian estimation	Point estimation	Doubly collapsed VI	[6]
	DGP	×	Discrete-layer	N/A	N/A	Point estimation	N/A	VI	[14]
David CD	DSVI-DGP	✓	Discrete-layer	N/A	Bayesian estimation	Point estimation	Point estimation	DSVI	[15]
Deep GP	SGHMC-DGP	✓	Discrete-layer	N/A	Bayesian estimation	Point estimation	Point estimation	SGHMC	[47]
	IPVI-DGP	✓	Discrete-layer	N/A	Bayesian estimation	Point estimation	Point estimation	IPVI	[48]
	NOVI-DGP	✓	Discrete-layer	N/A	Bayesian estimation	Point estimation	Point estimation	NOVI	[49]
G .: TI' CID	DIFFGP	✓	Continuous-layer	×	Bayesian estimation	Point estimation	Point estimation	SVI	[4]
Continuous-Time GP	Direct Matching of the FPK	✓	Continuous-layer	×	Bayesian estimation	Point estimation	Point estimation	Assumed density approximation	[50]
Ours	FB-DIFFGP	√	Continuous-layer	✓	Bayesian estimation	Bayesian estimation	Bayesian estimation	SVI + coupled neural SDEs	

TABLE I: Existing literature on sparse GPs, deep GPS and continuous-time GPs. We summarize the handling methods for the kernel hyperparameters λ , inducing points \mathbf{Z} , inducing variables \mathbf{U} , as well as their inference methods, whether through point estimation or Bayesian estimation.

framework and introducing SDEs to describe time evolution, DIFFGPs can learn continuous-time transformations or flows of the data. Based on [4], [50] derived direct approximations to the Fokker–Planck–Kolmogorov (FPK) equation in an assumed density Gaussian form that avoids sampling-based inference in the latent space, which makes inference fast. Our work builds upon the model proposed by [4] and combines it with the advantages of Fully Bayesian Gaussian processes. Additionally, we treat the hyperparameters as time-varying and utilize coupled neural SDEs for posterior inference of both the hyperparameters and inducing points. We summarize the previous methods in Table I.

d) SDE solvers: SDE solvers are numerical methods for approximating the state trajectories of the system over time by discretizing the SDEs into steps and iteratively updating the state variables. They are widely used in scientific and engineering fields, especially in computing Neural SDEs [51], [9], [8]. In Neural SDEs, the drift and diffusion terms of the SDE are parameterized using neural networks. This allows for more expressive modeling of the dynamics compared to traditional SDEs. SDE solvers are vital for training and inference in Neural SDE models. By approximating state trajectories, SDE solvers enable the calculation of gradients [7], [52], which is necessary for optimizing neural network parameters using techniques like stochastic gradient descent. Moreover, SDE solvers are also used in the simulation and generation of data from the learned Neural SDE models. These solvers enable the generation of synthetic data that captures the complex dynamics of the modeled systems, making it possible to analyze and explore the behavior of the neural system under different conditions. The use of SDE solvers in Neural SDEs has shown remarkable results in various machine learning applications including time series forecasting [53], generative modeling [54], uncertainty quantification, and reinforcement learning [55].

While our work indeed builds on the findings of [4], [7], [22], we have innovatively combined the methods of neural SDEs and variational inference to address the issue of kernel hyperparameter uncertainty in the DIFFGP model. Our empirical results provide strong evidence supporting our conclusions, demonstrating the effectiveness of our approach.

Dataset	method	MSE	NLL
Oilflow (1000,12)	Standard GPLVM	2.45(0.05)	-12.42(0.07)
	DIFFGP	1.87(0.04)	-14.41(0.04)
	FB-DIFFGP (Ours)	1.65(0.03)	-16.51(0.05)

TABLE II: MSE and NLL for our FB-DIFFGP compared to the baseline and standard GPLVM in toy datasets.

IV. EXPERIMENTS

In this section, we evaluate the performance of our proposed approximate inference method, FB-DIFFGP, on UCI datasets for regression and classification tasks. We compare it against state-of-the-art techniques like SVGP [11], DGP [15], and DIFFGP [4]. The number of inducing points M is manually selected, balancing accuracy and computation time. We optimize all parameters jointly using the evidence lower bound and employ stochastic optimization with mini-batches and the Adam optimizer. Numerical solutions of SDEs are obtained using the Euler-Maruyama solver with 20 time steps. The number of time steps changes if T is increased. For larger T, we would typically need to increase the number of time steps to maintain the same level of accuracy in the discretization of the SDE. This ensures that the solution remains precise and the numerical methods used are effective for longer time intervals. Other solvers, such as higher-order or adaptive methods, can also be easily implemented in Python toolkits.

Our model primarily handles classification and regression tasks, employing a simple network architecture with a few fully connected layers. The mini-batch size chosen is 10,000, and the learning rate is set to 0.01. We plan to compare more architectures in future work and explore their differences and applicability. Our implementation utilizes GPyTorch [34], a Gaussian processes framework based on PyTorch. For comparison, we used a simple two-layer BNN. The network consists of one hidden layer with a specified number of neurons, followed by an output layer. The DNN used for comparison is deployed as described in [57]. This network architecture includes several layers, with specifics provided in the paper.

A. Toy Dataset for Unsupervised Task

We applied our proposed model architecture to an unsupervised dimensionality reduction task using the Bayesian Gaussian Process Latent Variable Model (GPLVM) [58] for data reconstruction. Our toy dataset is the multi-phase Oilflow

		Yacht	Boston	Energy	Concrete	Power	Elevators	Protein	Year
	$N \\ D$	308 6	506 13	768 8	1,030 8	9,568 4	16,599 18	45,730 9	515,345 90
Linear		0.68(0.05)	4.24(0.16)	2.88(0.05)	10.54(0.13)	4.51(0.03)	5.08(0.03)	5.21(0.02)	6.35(0.05)
BNN	L=2	0.47(0.04)	3.01(0.18)	1.80(0.05)	5.67(0.09)	4.12(0.03)	4.57(0.03)	4.73(0.01)	5.78(0.05)
Sparse GP	M = 100 $M = 500$	0.45(0.04) 0.44(0.04)	2.87(0.15) 2.73(0.12)	0.78(0.02) 0.47(0.02)	5.97(0.11) 5.53(0.12)	3.91(0.03) 3.79(0.03)	4.47(0.03) 4.32(0.03)	4.43(0.03) 4.10(0.03)	5.59(0.06) 5.33(0.04)
Deep GP $M = 100$	L = 2 L = 3 L = 4 L = 5	0.45(0.03) 0.45(0.03) 0.44(0.03) 0.42(0.03)	2.90(0.17) 2.93(0.16) 2.90(0.15) 2.92(0.17)	0.47(0.01) 0.48(0.01) 0.48(0.01) 0.47(0.01)	5.61(0.10) 5.64(0.10) 5.68(0.10) 5.65(0.10)	3.79(0.03) 3.73(0.04) 3.71(0.04) 3.68(0.03)	4.35(0.04) 4.34(0.03) 4.32(0.03) 4.30(0.03)	4.00(0.03) 3.81(0.04) 3.74(0.04) 3.72 (0.04)	5.43(0.04) 5.38(0.04) 5.25(0.03) 5.23 (0.03)
DIFFGP $M = 100$	T = 1.0 T = 2.0 T = 3.0 T = 4.0 T = 5.0	0.45(0.04) 0.43(0.04) 0.43(0.03) 0.42(0.03) 0.40(0.04)	2.80(0.13) 2.68(0.10) 2.69(0.14) 2.67(0.13) 2.58(0.12)	0.49(0.02) 0.48(0.02) 0.47(0.02) 0.49(0.02) 0.50(0.02)	5.32(0.10) 4.96(0.09) 4.76(0.12) 4.65(0.12) 4.56(0.12)	3.76(0.03) 3.72(0.03) 3.68(0.03) 3.66(0.03) 3.65(0.03)	4.38(0.03) 4.33(0.03) 4.32(0.03) 4.30(0.03) 4.30(0.02)	4.04(0.04) 4.00(0.04) 3.92(0.04) 3.89(0.04) 3.87(0.04)	5.45(0.04) 5.41(0.03) 5.37(0.03) 5.33(0.03) 5.30(0.03)
FB-DIFFGP (ours) $M = 100$	T = 1.0 T = 2.0 T = 3.0 T = 4.0 T = 5.0	0.43 (0.04) 0.41 (0.03) 0.41 (0.03) 0.40 (0.02) 0.38 (0.04)	2.63 (0.10) 2.49 (0.10) 2.47 (0.11) 2.45 (0.09) 2.39 (0.10)	0.42 (0.01) 0.41 (0.02) 0.39 (0.01) 0.37 (0.02) 0.38 (0.01)	4.75 (0.12) 4.33 (0.11) 4.22 (0.12) 4.07 (0.11) 4.01 (0.11)	3.64 (0.03) 3.61 (0.03) 3.58 (0.03) 3.54 (0.03) 3.53 (0.03)	4.32 (0.03) 4.30 (0.03) 4.28 (0.04) 4.25 (0.03) 4.25 (0.02)	3.94 (0.03) 3.88 (0.03) 3.85 (0.03) 3.81 (0.03) 3.79 (0.03)	5.40 (0.04) 5.36 (0.03) 5.33 (0.03) 5.28 (0.03) 5.24 (0.03)

TABLE III: Test RMSE values of 8 benchmark datasets. Uses random 90% / 10% training and test splits, repeated 20 times.

		Yacht	Boston	Energy	Concrete	Power	Elevators	Protein	Year
	$N \\ D$	308 6	506 13	768 8	1,030 8	9,568 4	16,599 18	45,730 9	515,345 90
Linear		-0.72(0.03)	-2.89(0.03)	-2.48(0.02)	-3.78(0.01)	-2.93(0.01)	-2.76(0.03)	-3.07(0.00)	-6.32(0.03)
BNN	L=2	-0.64(0.06)	-2.57(0.09)	-2.04(0.02)	-3.16(0.02)	-2.84(0.01)	-2.45(0.05)	-2.97(0.00)	-5.62(0.03)
Sparse GP	M = 100 $M = 500$	-0.61(0.04) -0.57(0.03)	-2.47(0.05) -2.40(0.07)	-1.29(0.02) - 0.93(0.01)	-3.18(0.02) -3.09(0.02)	-2.75(0.01) -2.75(0.01)	-2.41(0.04) -2.26(0.04)	-2.91(0.00) -2.83(0.00)	-5.46(0.03) -5.38(0.03)
Deep GP $M = 100$	L = 2 L = 3 L = 4 L = 5	-0.61(0.05) -0.58(0.04) -0.60(0.04) -0.58(0.03)	-2.47(0.05) -2.49(0.05) -2.48(0.05) -2.49(0.05)	-0.73(0.02) -0.75(0.02) -0.76(0.02) -0.74(0.02)	-3.12(0.01) -3.13(0.01) -3.14(9.01) -3.13(0.01)	-2.75(0.01) -2.74(0.01) -2.74(0.01) -2.73(0.01)	-2.32(0.03) -2.28(0.03) -2.25(0.03) -2.24(0.03)	-2.81(0.00) -2.75(0.00) -2.73(0.00) -2.71(0.00)	-5.48(0.04) -5.42(0.04) -5.36(0.03) -5.34(0.03)
DIFFGP $M = 100$	T = 1.0 T = 2.0 T = 3.0 T = 4.0 T = 5.0	-0.57(0.04) -0.55(0.03) -0.53(0.03) -0.56(0.05) -0.54(0.03)	-2.36(0.04) -2.32(0.04) -2.31(0.05) -2.33(0.06) -2.30(0.05)	-0.65(0.03) -0.63(0.03) -0.63(0.03) -0.65(0.03) -0.66(0.03)	-3.05(0.02) -2.96(0.02) -2.93(0.04) -2.91(0.04) -2.90(0.05)	-2.75(0.01) -2.74(0.01) -2.72(0.01) -2.72(0.01) -2.72(0.01)	-2.30(0.03) -2.27(0.04) -2.25(0.04) -2.25(0.03) -2.26(0.02)	-2.79(0.04) -2.78(0.04) -2.79(0.00) -2.78(0.00) -2.77(0.00)	-5.40(0.04) -5.36(0.05) -5.31(0.04) -5.29(0.03) -5.28(0.03)
FB-DIFFGP (ours) $M = 100$	T = 1.0 T = 2.0 T = 3.0 T = 4.0 T = 5.0	-0.51(0.03) -0.49(0.03) -0.47(0.03) -0.44(0.04) -0.43(0.03)	-2.28(0.04) -2.26(0.05) -2.23(0.04) -2.21(0.05) -2.19(0.04)	-0.62(0.03) -0.59(0.03) -0.56(0.04) -0.54(0.03) -0.52(0.02)	-2.75(0.03) -2.72(0.03) -2.63(0.03) -2.63(0.04) -2.60(0.03)	-2.68(0.01) -2.66(0.01) -2.66(0.01) -2.63(0.02) -2.62(0.04)	-2.28(0.04) -2.26(0.04) -2.25(0.03) -2.24(0.04) -2.23(0.03)	-2.59(0.02) -2.58(0.02) -2.56(0.01) -2.57(0.01) -2.55(0.01)	-5.18(0.04) -5.16(0.03) -5.14(0.03) -5.13(0.04) -5.11(0.03)

TABLE IV: Test log likelihood values of 8 benchmark datasets. Uses random 90% / 10% training and test splits, repeated 20 times.

data [59], comprising 1,000 data points in 12 dimensions, categorized into three classes representing different phases of oil flow in a pipeline. We reduced the data's dimensionality to 10 while striving to retain as much information as possible. We report the reconstruction error and mean squared error (MSE) with ±2 standard errors across ten optimization runs. Since the training is unsupervised, the inherent ground-truth labels were not included in the training process. The 2D projections of the latent space for the Oilflow data clearly demonstrate that our model successfully uncovers the class structure. To emphasize the strengths of our model, we present the results of the 2D latent space for three models in Figure 4. As shown in Figure

4, the reconstructed data points for the three classes are more distinctly separated in our model, resulting in improved and more intuitive clustering. From Table II, we observe that our proposed FB-DIFFGP outperforms both the Standard GPLVM and DIFFGP methods, yielding lower reconstruction loss and improved uncertainty estimation.

B. UCI Regression Benchmarks

We compared our model against the state-of-the-art results reported in [4] on eight regression benchmarks. The datasets were tested with different flow time values ranging from 1 to 5.

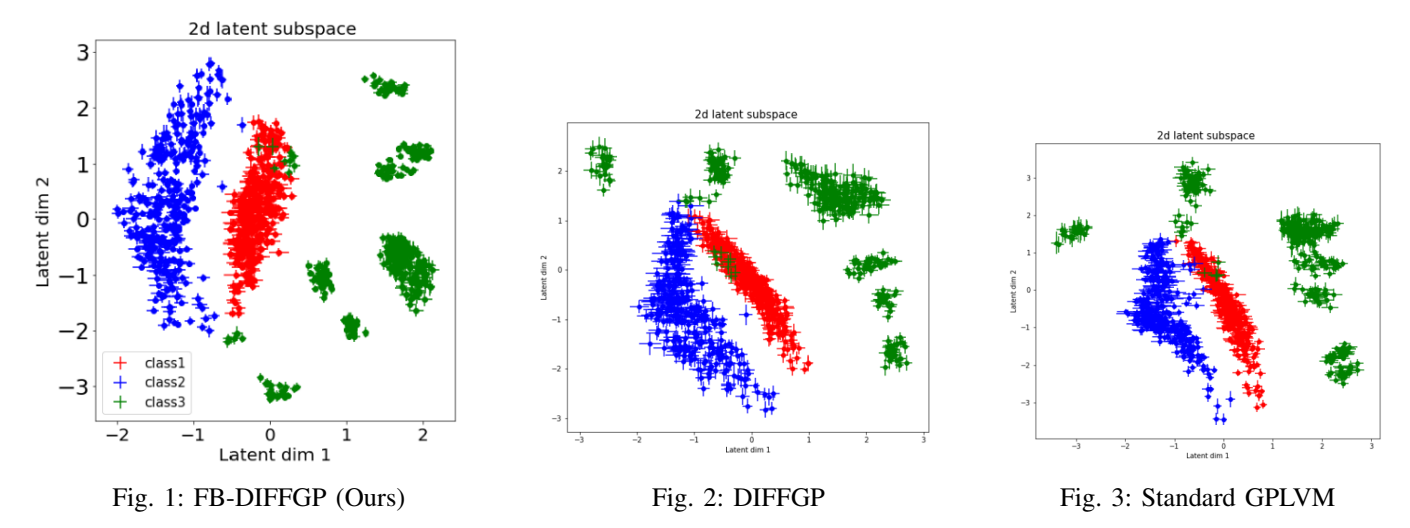


Fig. 4: The unsupervised dimensionality reduction task using GPLVM for data reconstruction

For both Gaussian Process methods, we used the RBF kernel with ARD and 100 inducing points. Each experiment was repeated 20 times with random 90% / 10% training and test splits. During testing, we computed the predictive mean and variance for each sample generated from (4), and calculated the average summary statistics, including RMSE and Log Likelihood (LL) across these samples. The mean and standard error of RMSE values were reported in Table III, while the mean and standard error of LL values were reported in the Table IV.

From Table III and Table IV, it is clear that our method outperforms previous methods on all eight datasets, with significant improvements observed on the boston, energy, concrete, and protein datasets. Our bolding strategy is aligned with the T hyperparameter in DIFFGP. We also observed a similar trend to [4], where increasing the flow time can increase the model capacity without overfitting, consequently improving the model's generalization ability.

a) Simulate kernel hyperparameter flows: To illustrate the improvement over the baseline more clearly, we simulated the trajectory of the learned kernel hyperparameters λ SDE. Since λ is indeed multivariate, we only displayed a slice of it. For visualization purposes, we selected the Concrete dataset and set T=10.0. The results are shown in Figure 5. The x-axis represents time t, while the y-axis represents the values of the hyperparameters. In order to facilitate the visualization of the trajectories of the SDE, we displayed 30 sample paths in the figure and selected fixed initial values for optimization purposes. From the plot, we can observe that the posterior of our kernel hyperparameters is no longer a point estimate but a posterior SDE flow. Our trajectories serve as illustrative representations of what the posterior SDE has learned, providing insight into the uncertainty estimation for the hyperparameters. The detailed uncertainty estimates are provided in the LL table IV. In Figure 6 and Figure 7, we respectively display the empirical distribution of these 100 paths at T = 10.0 using a histogram and a density curve plot.

- b) Computational efficiency: In a similar manner to the baseline algorithms, each training iteration of FB-DIFFGP requires computing the inverse covariance with a complexity of $\mathcal{O}(M^3)$. In Table V, we compare our method, FB-DIFFGP, with baseline DIFFGP trained for a fixed epoch. The experiment is repeated five times on the same fold, and the results are averaged. Each run is conducted on a dedicated instance in a cloud computing platform equipped with a single Tesla A100 GPU. The results demonstrate that FB-DIFFGP does not significantly increase computational costs, thanks to the efficient parallel processing capabilities of deep learning GPUs.
- c) Comparison for the proposed algorithm with different numbers of inducing points.: We compared the performance of our proposed algorithm with M=100 and M=500 inducing points in Table VI. Our findings indicate that, similar to classical sparse GP methods, the performance improves with a higher number of inducing points, resulting in lower RMSE values. However, this improvement comes at the cost of increased training time, as the computational complexity grows with the number of inducing points.

C. UCI Classification Benchmarks

As a large-scale example, we conducted experiments on the Higgs dataset, which consists of 11 million data points with 28 features. This dataset was generated through Monte Carlo simulations of particle dynamics in accelerators for Higgs boson detection. We randomly allocated 90% of the data for training and kept the remaining 10% for testing. To evaluate the performance, we utilized the area under the curve (AUC) metric and compared our results with previously reported methods. Table VII presents the obtained test performance, demonstrating that our FB-DIFFGP method outperforms the competing approaches. Additionally, we conducted experiments on the SUSY dataset, and the results showcased the competitive performance of our proposed algorithm.

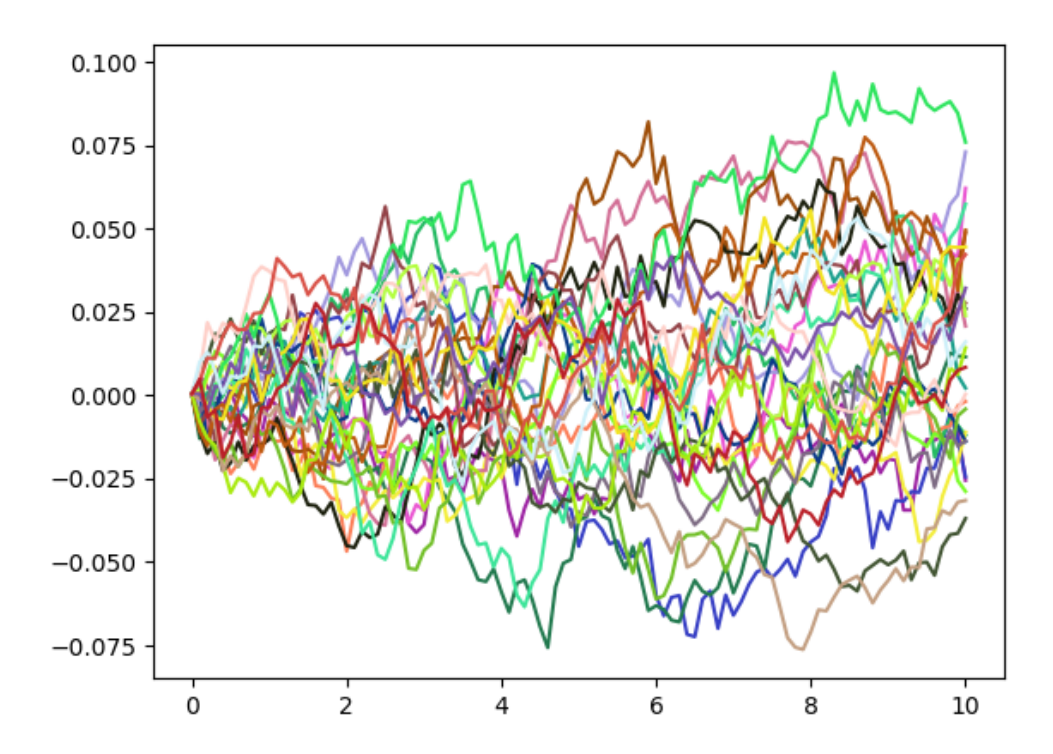


Fig. 5: In the figure for the Concrete dataset, we displayed 30 sample paths to visualize the trajectories of the SDE. The plot shows that the posterior of our kernel hyperparameters is not a point estimate but a posterior SDE flow. The diffusion process shown in this figure is multivariate, but we only displayed a slice of it in the two-dimensional plot. The x-axis represents time t, while the y-axis represents the values of the hyperparameters.

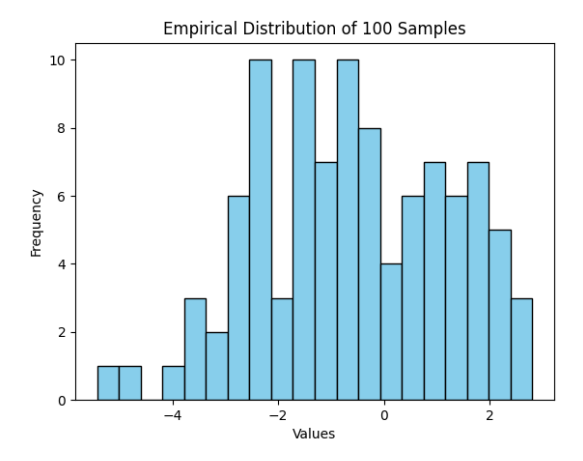


Fig. 6: Empirical histogram of 100 sample paths at time T=10.0 for Concrete dataset. The x-axis represents the values of the kernel parameters, and the y-axis shows the empirical distribution

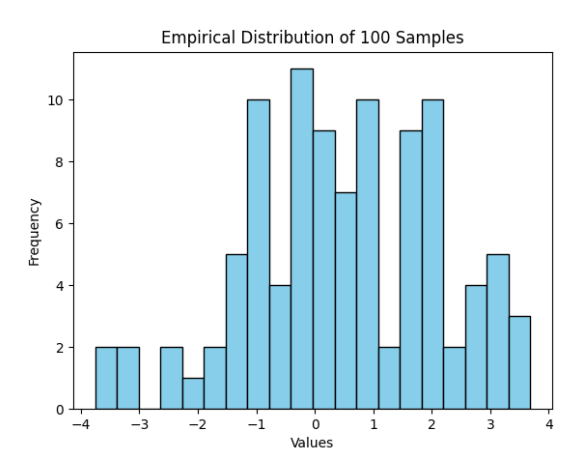


Fig. 7: Empirical histogram of 100 sample paths at time T=10.0 for Energy dataset. The x-axis represents the values of the kernel parameters, and the y-axis shows the empirical distribution

	Yacht	Boston	Energy	Concrete	Power	Elevators	Protein	Year
$N \\ D$	308 6	506 13	768 8	1,030 8	9,568 4	16,599 18	45,730 9	515,345 90
DIFFGP $M = 100, T = 1$	0.59s	0.61s	0.62s	0.70s	2.34s	3.85s	11.69s	120.65s
FB-DIFFGP (ours) $M = 100, T = 1$	0.61s	0.64s	0.66s	0.75s	2.45s	4.03s	12.87s	126.87s

TABLE V: The proposed algorithm compared to the baseline model in terms of runtime: the time required to complete one full pass of the entire dataset, also known as one epoch.

		Yacht	Boston	Energy	Concrete	Power	Elevators	Protein	Year
	D	308 6	506 13	768 8	1,030 8	9,568 4	16,599 18	45,730 9	515,345 90
FB-DIFFGP (ours) $M = 100$		0.43(0.04)	2.63(0.10)	0.42(0.01)	4.75(0.12)	3.64(0.03)	4.32(0.03)	3.94(0.03)	5.40(0.04)
FB-DIFFGP (ours) $M = 500$		0.42(0.04)	2.52(0.07)	0.40(0.01)	4.46(0.14)	3.62(0.03)	4.29(0.03)	3.86(0.03)	5.38(0.03)

TABLE VI: Comparison of RMSE for the proposed algorithm with different numbers of inducing points M.

		SUSY	HIGGS
	N	5,500,000	11,000,000
	D	18	28
DNN		0.876	0.885
Cmana CD	M = 100	0.875	0.785
Sparse GP	M = 500	0.876	0.794
	L=2	0.877	0.830
Deep GP	L = 3	0.877	0.837
M = 100	L = 4	0.877	0.841
	L = 5	0.877	0.846
DIFFGP	T = 1.0	0.878	0.840
M = 100	T = 3.0	0.878	0.841
	T = 5.0	0.878	0.842
FB-DIFFGP(ours)	T = 1.0	0.887	0.852
M = 100	T = 3.0	0.887	0.856
	T = 5.0	0.887	0.857

TABLE VII: Test AUC values for large-scale classification datasets. Uses random 90% / 10% training and test splits.

V. CONCLUSION

Our research introduces a cutting-edge fully Bayesian approach that treats kernel hyperparameters as random variables and utilizes interconnected stochastic differential equations (SDEs) to infer the posterior distribution of DIFFGPs. By capturing uncertainty in hyperparameter estimation, our method significantly enhances model adaptability in capturing complex system dynamics. Through compelling experimental results, we demonstrate the superiority of our methodology over conventional techniques, showcasing improved performance in flexibility and accuracy. This research opens doors for advancements in Bayesian inference and provides a powerful tool for modeling continuous-time Gaussian processes. Future exploration includes expanding the application of our FB-DIFFGP model in diverse domains such as image analysis and financial datasets, offering exciting opportunities for further discovery in probabilistic modeling.

REFERENCES

- [1] C. E. Rasmussen, "Gaussian processes in machine learning," in *Summer school on machine learning*. Springer, 2003, pp. 63–71.
- [2] D. Duvenaud, O. Rippel, R. Adams, and Z. Ghahramani, "Avoiding pathologies in very deep networks," in *Artificial Intelligence and Statis*tics. PMLR, 2014, pp. 202–210.
- [3] M. M. Dunlop, M. A. Girolami, A. M. Stuart, and A. L. Teckentrup, "How deep are deep gaussian processes?" *Journal of Machine Learning Research*, vol. 19, no. 54, pp. 1–46, 2018.
- [4] P. Hegde, M. Heinonen, H. Lähdesmäki, and S. Kaski, "Deep learning with differential gaussian process flows," arXiv preprint arXiv:1810.04066, 2018.
- [5] V. Lalchand and C. E. Rasmussen, "Approximate inference for fully bayesian gaussian process regression," in *Symposium on Advances in Approximate Bayesian Inference*. PMLR, 2020, pp. 1–12.
- [6] V. Lalchand, W. Bruinsma, D. Burt, and C. E. Rasmussen, "Sparse gaussian process hyperparameters: Optimize or integrate?" Advances in Neural Information Processing Systems, vol. 35, pp. 16612–16623, 2022
- [7] X. Li, T.-K. L. Wong, R. T. Chen, and D. Duvenaud, "Scalable gradients for stochastic differential equations," in *International Conference on Artificial Intelligence and Statistics*. PMLR, 2020, pp. 3870–3882.
- [8] X. Liu, T. Xiao, S. Si, Q. Cao, S. Kumar, and C.-J. Hsieh, "How does noise help robustness? explanation and exploration under the neural sde framework," in *Proceedings of the IEEE/CVF Conference on Computer Vision and Pattern Recognition*, 2020, pp. 282–290.
- [9] L. Kong, J. Sun, and C. Zhang, "Sde-net: Equipping deep neural networks with uncertainty estimates," arXiv preprint arXiv:2008.10546, 2020.
- [10] B. Tzen and M. Raginsky, "Neural stochastic differential equations: Deep latent gaussian models in the diffusion limit," arXiv preprint arXiv:1905.09883, 2019.
- [11] J. Hensman, A. Matthews, and Z. Ghahramani, "Scalable variational gaussian process classification," in *Artificial Intelligence and Statistics*. PMLR, 2015, pp. 351–360.
- [12] J. Hensman, A. G. Matthews, M. Filippone, and Z. Ghahramani, "Mcmc for variationally sparse gaussian processes," Advances in Neural Information Processing Systems, vol. 28, 2015.
- [13] C. Yildiz, M. Heinonen, J. Intosalmi, H. Mannerstrom, and H. Lahdesmaki, "Learning stochastic differential equations with gaussian processes without gradient matching," in 2018 IEEE 28th International Workshop on Machine Learning for Signal Processing (MLSP). IEEE, 2018, pp.
- [14] A. Damianou and N. D. Lawrence, "Deep gaussian processes," in Artificial intelligence and statistics. PMLR, 2013, pp. 207–215.
- [15] H. Salimbeni and M. Deisenroth, "Doubly stochastic variational inference for deep gaussian processes," Advances in neural information processing systems, vol. 30, 2017.
- [16] T. Zhang, Z. Yao, A. Gholami, J. E. Gonzalez, K. Keutzer, M. W. Mahoney, and G. Biros, "Anodev2: A coupled neural ode framework," Advances in Neural Information Processing Systems, vol. 32, 2019.

- [17] K. O. Stanley, D. B. D'Ambrosio, and J. Gauci, "A hypercube-based encoding for evolving large-scale neural networks," *Artificial life*, vol. 15, no. 2, pp. 185–212, 2009.
- [18] J. Koutnik, F. Gomez, and J. Schmidhuber, "Evolving neural networks in compressed weight space," in *Proceedings of the 12th annual conference* on Genetic and evolutionary computation, 2010, pp. 619–626.
- [19] D. Ha, A. M. Dai, and Q. V. Le, "Hypernetworks," CoRR, vol. abs/1609.09106, 2016. [Online]. Available: http://arxiv.org/abs/1609. 09106
- [20] Y. Kim, S. Wiseman, A. Miller, D. Sontag, and A. Rush, "Semi-amortized variational autoencoders," in *International Conference on Machine Learning*. PMLR, 2018, pp. 2678–2687.
- [21] A. Agrawal and J. Domke, "Amortized variational inference for simple hierarchical models," *Advances in Neural Information Processing* Systems, vol. 34, pp. 21388–21399, 2021.
- [22] M. Opper, "Variational inference for stochastic differential equations," Annalen der Physik, vol. 531, no. 3, p. 1800233, 2019.
- [23] P. Kidger, J. Foster, X. Li, and T. J. Lyons, "Neural sdes as infinite-dimensional gans," in *International conference on machine learning*. PMLR, 2021, pp. 5453–5463.
- [24] W. Xu, R. T. Chen, X. Li, and D. Duvenaud, "Infinitely deep bayesian neural networks with stochastic differential equations," in *International Conference on Artificial Intelligence and Statistics*. PMLR, 2022, pp. 721–738
- [25] N. G. Van Kampen, "Stochastic differential equations," *Physics reports*, vol. 24, no. 3, pp. 171–228, 1976.
- [26] M. Boué and P. Dupuis, "A variational representation for certain functionals of brownian motion," *The Annals of Probability*, vol. 26, no. 4, pp. 1641–1659, 1998.
- [27] D. J. Rezende, S. Mohamed, and D. Wierstra, "Stochastic backpropagation and approximate inference in deep generative models," in International conference on machine learning. PMLR, 2014, pp. 1278– 1286
- [28] S.-i. Amari, "Backpropagation and stochastic gradient descent method," Neurocomputing, vol. 5, no. 4-5, pp. 185–196, 1993.
- [29] M. D. Hoffman, D. M. Blei, C. Wang, and J. Paisley, "Stochastic variational inference," *Journal of Machine Learning Research*, 2013.
- [30] J. Schreiter, P. Englert, D. Nguyen-Tuong, and M. Toussaint, "Sparse gaussian process regression for compliant, real-time robot control," in 2015 IEEE International Conference on Robotics and Automation (ICRA). IEEE, 2015, pp. 2586–2591.
- [31] G.-L. Tran, E. V. Bonilla, J. Cunningham, P. Michiardi, and M. Filippone, "Calibrating deep convolutional gaussian processes," in *The 22nd International Conference on Artificial Intelligence and Statistics*. PMLR, 2019, pp. 1554–1563.
- [32] A. G. d. G. Matthews, M. Van Der Wilk, T. Nickson, K. Fujii, A. Boukouvalas, P. León-Villagrá, Z. Ghahramani, and J. Hensman, "Gpflow: A gaussian process library using tensorflow." *J. Mach. Learn. Res.*, vol. 18, no. 40, pp. 1–6, 2017.
- [33] K. Krauth, E. V. Bonilla, K. Cutajar, and M. Filippone, "Autogp: Exploring the capabilities and limitations of gaussian process models," arXiv preprint arXiv:1610.05392, 2016.
- [34] J. Gardner, G. Pleiss, K. Q. Weinberger, D. Bindel, and A. G. Wilson, "Gpytorch: Blackbox matrix-matrix gaussian process inference with gpu acceleration," *Advances in neural information processing systems*, vol. 31, 2018.
- [35] M. Titsias, "Variational learning of inducing variables in sparse gaussian processes," in *Artificial intelligence and statistics*. PMLR, 2009, pp. 567–574.
- [36] M. Lázaro-Gredilla and A. Figueiras-Vidal, "Inter-domain gaussian processes for sparse inference using inducing features," Advances in Neural Information Processing Systems, vol. 22, 2009.
- [37] M. Van der Wilk, C. E. Rasmussen, and J. Hensman, "Convolutional gaussian processes," Advances in Neural Information Processing Systems, vol. 30, 2017.
- [38] P. Li and S. Chen, "A review on gaussian process latent variable models," CAAI Transactions on Intelligence Technology, vol. 1, no. 4, pp. 366–376, 2016.
- [39] G. Corani, A. Benavoli, and M. Zaffalon, "Time series forecasting with gaussian processes needs priors," in *Joint European Conference on Machine Learning and Knowledge Discovery in Databases*. Springer, 2021, pp. 103–117.
- [40] J. Bernardo, J. Berger, A. Dawid, A. Smith et al., "Regression and classification using gaussian process priors," *Bayesian statistics*, vol. 6, p. 475, 1998.
- [41] C. Williams and C. Rasmussen, "Gaussian processes for regression," Advances in neural information processing systems, vol. 8, 1995.

- [42] D. Barber and C. Williams, "Gaussian processes for bayesian classification via hybrid monte carlo," *Advances in neural information processing* systems, vol. 9, 1996.
- [43] I. Murray and R. P. Adams, "Slice sampling covariance hyperparameters of latent gaussian models," Advances in neural information processing systems, vol. 23, 2010.
- [44] G. P. Models-GPM, "A comparative evaluation of stochastic-based inference methods for gaussian process models."
- [45] T. D. Bui, C. Nguyen, and R. E. Turner, "Streaming sparse gaussian process approximations," Advances in Neural Information Processing Systems, vol. 30, 2017.
- [46] S. Rossi, M. Heinonen, E. Bonilla, Z. Shen, and M. Filippone, "Sparse gaussian processes revisited: Bayesian approaches to inducing-variable approximations," in *International Conference on Artificial Intelligence* and Statistics. PMLR, 2021, pp. 1837–1845.
- [47] M. Havasi, J. M. Hernández-Lobato, and J. J. Murillo-Fuentes, "Inference in deep gaussian processes using stochastic gradient hamiltonian monte carlo," *Advances in neural information processing systems*, vol. 31, 2018.
- [48] H. Yu, Y. Chen, B. K. H. Low, P. Jaillet, and Z. Dai, "Implicit posterior variational inference for deep gaussian processes," *Advances in neural* information processing systems, vol. 32, 2019.
- [49] J. Xu, S. Du, J. Yang, Q. Ma, and D. Zeng, "Neural operator variational inference based on regularized stein discrepancy for deep gaussian processes," *arXiv* preprint arXiv:2309.12658, 2023.
- [50] A. Solin, E. Tamir, and P. Verma, "Scalable inference in sdes by direct matching of the fokker–planck–kolmogorov equation," Advances in Neural Information Processing Systems, vol. 34, pp. 417–429, 2021.
- [51] X. Liu, T. Xiao, S. Si, Q. Cao, S. Kumar, and C.-J. Hsieh, "Neural sde: Stabilizing neural ode networks with stochastic noise," arXiv preprint arXiv:1906.02355, 2019.
- [52] P. Kidger, J. Foster, X. C. Li, and T. Lyons, "Efficient and accurate gradients for neural sdes," Advances in Neural Information Processing Systems, vol. 34, pp. 18747–18761, 2021.
- [53] L. Yang, T. Gao, Y. Lu, J. Duan, and T. Liu, "Neural network stochastic differential equation models with applications to financial data forecasting," *Applied Mathematical Modelling*, vol. 115, pp. 279–299, 2023.
- [54] J. Ho, A. Jain, and P. Abbeel, "Denoising diffusion probabilistic models," Advances in neural information processing systems, vol. 33, pp. 6840–6851, 2020.
- [55] T. Chen, L. Cheng, Y. Liu, W. Jia, and S. Ma, "Incremental reinforcement learning—a new continuous reinforcement learning frame based on stochastic differential equation methods," arXiv preprint arXiv:1908.02974, 2019.
- [56] T. D. Bui, C. V. Nguyen, S. Swaroop, and R. E. Turner, "Partitioned variational inference: A unified framework encompassing federated and continual learning," arXiv preprint arXiv:1811.11206, 2018.
- [57] P. Baldi, P. Sadowski, and D. Whiteson, "Searching for exotic particles in high-energy physics with deep learning," *Nature communications*, vol. 5, no. 1, p. 4308, 2014.
- [58] M. Titsias and N. D. Lawrence, "Bayesian gaussian process latent variable model," in *Proceedings of the thirteenth international conference on artificial intelligence and statistics*. JMLR Workshop and Conference Proceedings, 2010, pp. 844–851.
- [59] C. M. Bishop and G. D. James, "Analysis of multiphase flows using dualenergy gamma densitometry and neural networks," *Nuclear Instruments* and Methods in Physics Research Section A: Accelerators, Spectrometers, Detectors and Associated Equipment, vol. 327, no. 2-3, pp. 580– 593, 1993.